Transparent Copolyester/Organoclay Nanocomposites Prepared by In Situ Intercalation Polymerization: Synthesis, Characterization, and Properties

Yuhsin Tsai,[1] Cheng-Hsing Fan,[2] Chi-Yuan Hung,[2] Fuu-Jen Tsai[1,3]
[1]*School of Chinese Medicine, China Medical University, Taichung, Taiwan*

[2]*Nano-Powder and Thin Film Technology Center, Industrial Technology Research Institute, Tainan, Taiwan*

[3]*Department of Medical Genetics, Pediatrics and Medical Research, China Medical University Hospital, Taichung, Taiwan*

In this study, amorphous poly(ethylene terephthalate-*co*-1,3/1,4-cyclohexylenedimethylene terephthalate) (PETG)/organoclay nanocomposites was synthesized by the in situ intercalation polymerization of terephthalic acid, ethylene glycol, 1,3/1,4-cyclohexanedimethanol, and organoclay. The organoclay was obtained by modifying sodium montmorillonite (clay) with hexadecyl triphenylphosphonium bromide. The thermal, mechanical, optical, and gas barrier properties of these PETG nanocomposites with various organoclay contents (0–3 wt%) were discussed. The differential scanning calorimetry and X-ray analyses revealed that all of the nanocomposites were amorphous. X-ray diffraction and transmission electron micrographs showed that the organoclay was well dispersed in the polymer matrix, although some parts of the agglomerated layers remained on the scale of several hundreds of nanometers. The thermal stability and the mechanical property of the nanocomposites increased with organoclay content. The optical transmittances of nanocomposites that contained 0.5, 1, and 3 wt% of organoclay were 86.8%, 84.4%, and 77.4%, respectively. The oxygen transmission rate of the nanocomposite that contained 3 wt% of organoclay was about 50% of the PETG base polymer. POLYM. COMPOS., 32:89–96, 2011. © 2010 Society of Plastics Engineers

INTRODUCTION

Polymer/layered silicate nanocomposites have been extensively studied because the complete dispersion of layered silicate in a polymer optimizes the number of available reinforcing elements, subsequently improving many properties. For gas barrier properties, the layered silicate in the nanocomposites forces a penetrating molecule to diffuse through the nanocomposite in a tortuous pathway, which reduces the gas permeability of the nanocomposite [1, 2]. Furthermore, since the layered silicate is dispersed on the nanometer scale, the transparency of nanocomposites of amorphous polymers, such as poly(amic acid) [3], poly(methyl methacrylate) [4], polybutadiene [5], and UV-curing oligomer [6, 7], can be maintained close to that of the base polymer.

Glycol-modified poly(ethylene terephthalate) (PET) copolyester, generally poly(ethylene terephthalate-*co*-1,4-cyclohexylenedimethylene terephthalate) (PETG), is an amorphous thermoplastic of the commercial PET family and has a glass transition temperature (T_g) of about 80°C, similar to PET [8–10]. Because of its transparency, PETG is used in medical, pharmaceutical, and cosmetic packaging. Recently, few studies of PETG/layered silicate nanocomposites have been published. Kalgaonkar et al. [11–14] investigated how the intercalant affected the viscoelastic properties of the PETG/layered silicate nanocomposites, which were prepared by melt blending organically modified montmorillonites with PETG. Ranade et al. [15] also adopted the melt blending method to prepare PETG/montmorillonite nanocomposites and studied the effects of surfactant concentrations on the dispersion of montmorillonite in PETG matrix. Couderc et al. [16] studied the relaxation of PETG/montmorillonite nanocomposites by dielectric methods.

Among these investigations, none addresses the effect of layered silicate on both the gas barrier and optical properties of the PETG/montmorillonite nanocomposites, although the dispersed layered silicate in the amorphous PETG may improve its gas barrier without sacrificing its optical properties. It is especially useful for packaging

Correspondence to: Yuhsin Tsai; e-mail: yhtsai@mail.cmu.edu.tw
DOI 10.1002/pc.21021
Published online in Wiley Online Library (wileyonlinelibrary.com).

applications, which require transparency and clarity. This improvement is an important means in which the amorphous PETG nanocomposite differs from the crystalline PET nanocomposite. The rate of crystallization of PET/layered silicate nanocomposites exceeds that of PET [17–20], in which the added silicate is believed to act as a nucleating agent, and the PET/layered silicate nanocomposites are generally opaque.

This study evaluates how the layered silicate affects the gas barrier, the optical transparency, the physical, and the thermal properties of PETG nanocomposites by preparing a new PETG/layered silicate nanocomposite via in situ intercalation polymerization. The PETG/layered silicate nanocomposites were synthesized from terephthalic acid (TPA), ethylene glycol (EG), 1,3/1,4-cyclohexanedimethanol (CHDM), and organoclay. The organoclay were obtained by treating sodium montmorillonite with thermally stable intercalation agent, hexadecyl triphenylphosphonium bromide (HB), to prevent thermodegadation at high temperature during the polymerization [21–25]. The effects of various amounts of organoclay on the dispersion, crystallization, mechanical, thermal, optical, and gas transport properties of the nanocomposites were also examined in detail.

EXPERIMENTAL PROCEDURES

Materials

Terephthalic acid (98%), ethylene glycol (99+%), trifluoroacetic acid (TFA), phenol, tetrachloroethane, cobalt acetate ($Co(OAc)_2$), and tetrabutyl titanate ($Ti(O(CH_2)_3CH_3)_4$) were purchased from Aldrich. The 1,3/1,4-CHDM, which was an equilibrium mixture of 1,4-trans/1,4-cis/1,3-trans/1,3-cis (29.1/13.3/30.9/26.7), was purchased from Dow Chemical Company. Sodium montmorillonite (Kunipia F®, clay) with a cationic exchange capacity of 115 meq/100 g was purchased from Kunimine Company (Japan). The intercalation agent, hexadecyl triphenylphosphonium bromide (98+%), was purchased from Alfa Aesar Company. All of these chemicals were used as received without further purification.

Preparation of Organoclay

The organoclay was synthesized using an ion exchange reaction between sodium montmorillonite and HB [23, 24]. A 10 g mass of clay was added to 1,000 ml of distilled water. The dispersion was heated to 60°C and mechanically stirred for 8 h. The optimal weight of HB (HB/clay = 1/1 by equivalent) was added to the dispersion; the resultant mixture was stirred at 60°C for 48 h. The solution was filtered and the organoclay was washed thoroughly in an alcohol/water mixture (1:9, w:w) and distilled water three times to remove the residual salt. The organoclay was then dried overnight in a vacuum oven at 50°C. Figure 1 presents the FTIR spectra of HB, clay, and organoclay.

Preparation of PETG/Organoclay Nanocomposites

All of the polymers were prepared by two-stage melt polycondensation (esterification and polycondensation) in an autoclave reactor. The details of the synthesis can be found elsewhere [26, 27]. In the preparations, the reaction mixtures comprised excess EG (molar ratio of EG/TPA = 1.1), 1,3/1,4-CHDM (molar ratio of 1,3/1,4-CHDM/TPA = 0.3), TPA, various proportions of organoclay (0, 0.5, 1, and 3 wt%), 350 ppm $Ti(O(CH_2)_3CH_3)_4$, and 90 ppm $Co(OAc)_2$ by weight. The reaction mixture was heated to the final temperature (220–250°C) in an atmosphere of nitrogen. This first step was considered to have been completed after 4 h, when the theoretical amount of water was collected. In the second step, a vacuum (5 Torr) was applied slowly over a period (of about 30 min) to avoid excessive foaming and to minimize oligomer sublimation, which was a potential problem during melt polycondensation. The temperature increased (250–280°C) with the strength of the vacuum. The polycondensation was continued for about 2.5 h as the viscosity of the melt increased. After the polycondensation reaction was completed, the product was obtained from the autoclave reactor. All samples were ground in a mill, sieved, washed with methanol, and dried at 60°C for 24 h at reduced pressure. Table 1 present the preparation and the compositions of the PETG nanocomposites described in this work, respectively.

Characterization

The intrinsic viscosities of the polymers were measured using an Ubbelohde viscometer at 25°C in a mixture of phenol and tetrachloroethane (60:40, w:w). The ^1H NMR spectrum was obtained on a Bruker DRX-400 spectrometer at 25°C and 400 MHz. Duterated trifluoroacetic acid was used as a solvent.

Transmission electron micrographs (TEM) of PETG nanocomposites were obtained using a Hitachi H-7500 with an acceleration voltage of 120 kV. The specimens were prepared using an ultrathin microtome. Thin sections with a thickness of about 100 nm were cut using a diamond knife at 30°C. Fourier transform infrared spectroscopy (FTIR) spectra of samples were recorded on a Horiba FT-730 FTIR spectrometer. The samples were prepared by grinding a few milligrams of clay with 50 mg of KBr and pressing it into a thin film. The FTIR detection range was 400 to 4,000 cm^{-1}.

Thermal characterization was performed in an atmosphere of dry nitrogen using a differential scanning calorimeter (DSC) (Seiko SSC-5200). Both temperature and heat flow were calibrated using indium and tin standards. In the DSC measurement, a polymer sample (3.0–5.0 mg) was preheated at 300°C for 10 min to remove its thermal history, and then cooled to 0°C at a rate of 20°C/min.

 DOI 10.1002/pc

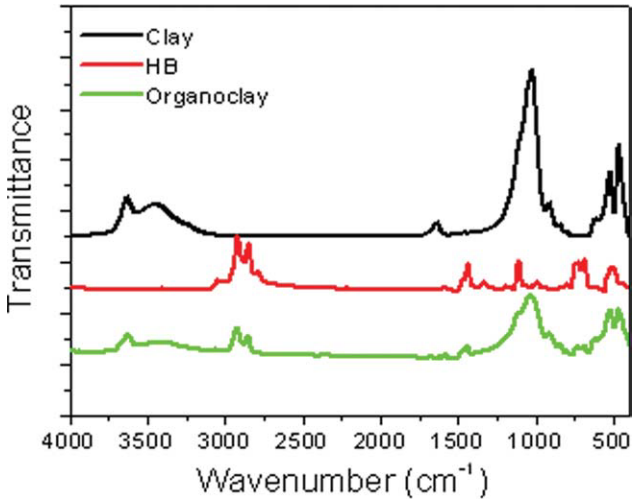

FIG. 1. FTIR spectra of HB, clay, and organoclay. [Color figure can be viewed in the online issue, which is available at wileyonlinelibrary.com.]

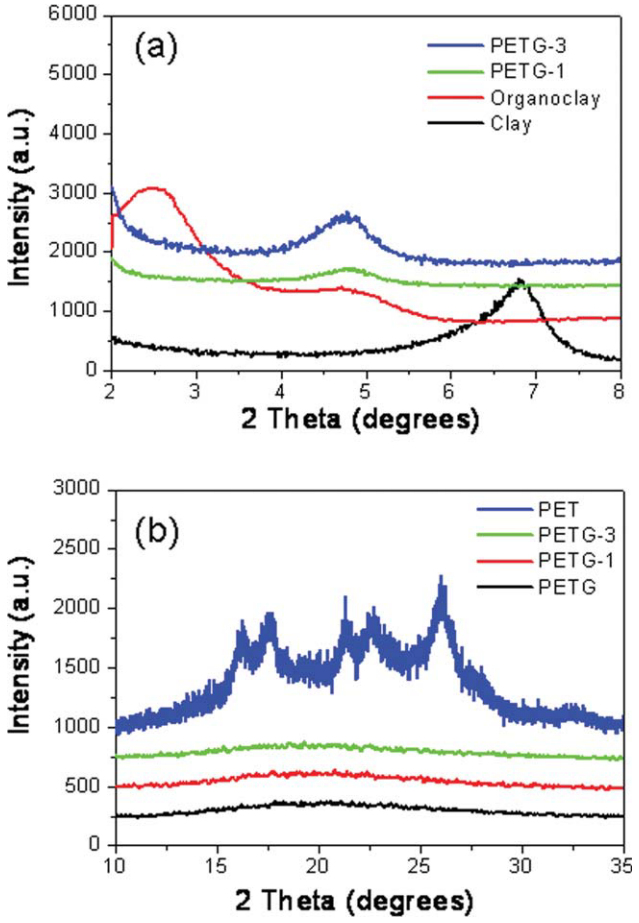

FIG. 2. XRD patterns of (a) clay, organoclay, and PETG nanocomposites; (b) PET, PETG, and PETG nanocomposites. [Color figure can be viewed in the online issue, which is available at wileyonlinelibrary.com.]

Next, the cooled sample was heated to 300°C at a rate of 20°C/min. T_m (melting temperature) and T_c (crystallization temperature) were the peak temperatures measured in the transitions in the heating run and the cooling run, respectively. T_g was the temperature at the middle point of the glass transition in the heating run. Thermogravimetric analysis (TGA) was performed using a Seiko Exstar-6000 thermobalance at a heating rate of 20°C/min in an atmosphere of nitrogen.

The samples used in gas transport analyses and the UV ray transmittance test were prepared from the glassy, unoriented, and amorphous film (thickness, 0.5 mm), which was obtained by melt compression followed by immersion in ice-cold water. The UV ray transmittance of the polymers was measured on a Labsphere UV-1000F ultraviolet spectrophotometer to characterize the UV radiation transmittance of the polymers. Oxygen transmission rate (OTR) of samples was measured at 40°C, a relative humidity of 0% and a flow rate of 10 cm^3/min using a Mocon OX-TRAN Model 2/61 universal apparatus [2, 17].

The samples for X-ray analyses were annealed at 120°C for 8 h. X-ray analyses were performed using a Siemens D-500 diffractometer with Ka-Cu radiation at a

TABLE 1. Compositions, viscosities, and thermal properties of nanocomposites.

Sample	Organoclay (wt%)	Composition[a] TPA/EG/CHDM (mol%)	Composition[b] TPA/EG/CHDM (mol%)	Viscosity[c] IV (dl/g)	Thermal properties T_g[d] (°C)	T_m[e] (°C)	T_{ch}[e] (°C)	T_{cc}[e] (°C)	T_d[f] (°C)	W_r[g] (%)
PETG	0	100/70/30	100/71.0/29.0	0.63	77.4	–	–	–	398	6.8
PETG-0.5	0.5	100/70/30	100/71.1/28.9	0.62	77.4	–	–	–	399	7.0
PETG-1	1.0	100/70/30	100/70.9/29.1	0.62	77.7	–	–	–	402	7.3
PETG-3	3.0	100/70/30	100/71.0/29.0	0.60	77.2	–	–	–	404	8.1

[a] Theoretical composition.
[b] Determined from ^{1}H NMR spectra.
[c] Intrinsic viscosity (dl/g) measured at 25°C in a phenol/tetrachloroethane mixture (60:40, w:w).
[d] T_g was obtained from the inflection point of the DSC traces of the melt-quenched samples during heating at 20°C/min.
[e] T_m and T_c of the pristine samples, measured by DSC at heating/cooling rate of 20°C/min.
[f] Temperature at which TGA traces recorded at a heating rate of 20°C/min revealed a 10% weight loss.
[g] Weight percentage of residue at 800°C.

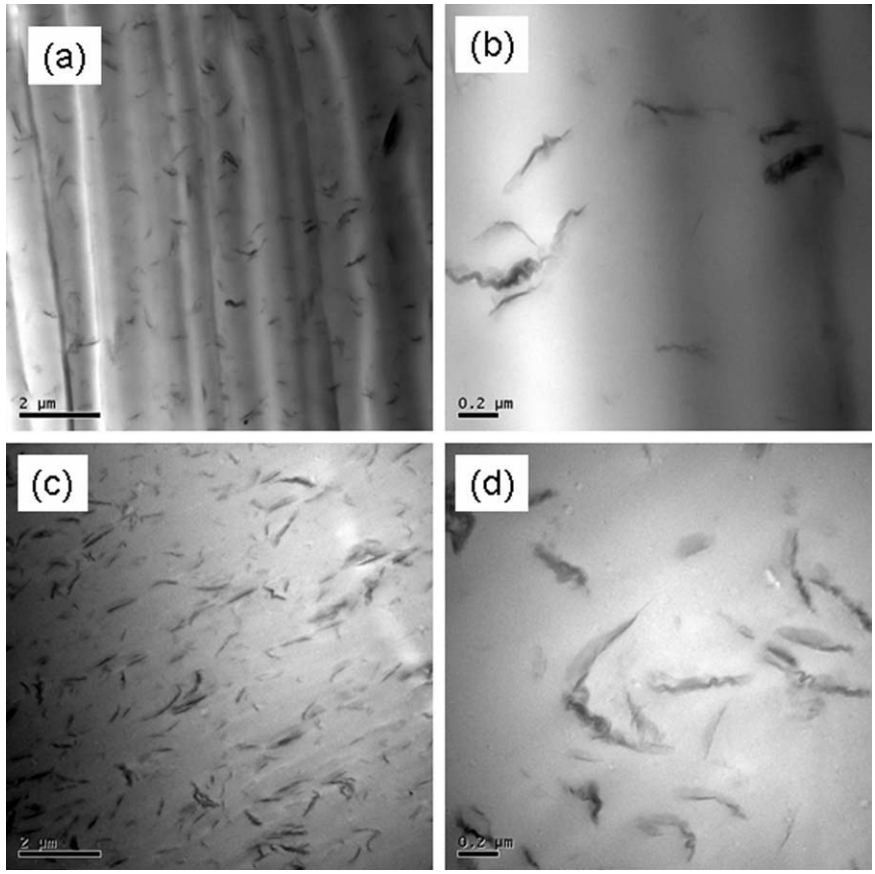

FIG. 3. TEM photographs of (a) PETG-1 ×10,000; (b) PETG-1 ×50,000; (c) PETG-3 ×10,000; and (d) PETG-3 ×50,000.

wavelength of 1.5418 Å. All polymers were injection-molded into unheated molds in an injection-molding machine to yield specimens for tensile tests and dynamic mechanical tests. The tensile mechanical properties were measured according to the ASTM D 638 standard for injection-molded specimens. The drawing speed in the tests was 20 mm/min using a Cometech QC-506 universal testing machine. The presented mechanical properties were averages of five tests. Dynamic mechanical analysis (DMA) was conducted on a TA-2980 in a tensile mode with a frequency of 1 Hz. Specimens were heated from 35 to 160°C at a rate of 5°C/min.

RESULTS AND DISCUSSION

Synthesis of Organoclay and Nanocomposites

Organoclay was synthesized using an ion exchange reaction between sodium montmorillonite and HB at 60°C for 48 h, followed by a washing workout to remove the residual salt. Figure 1 shows the FTIR spectra of HB, clay, and organoclay. The spectrum of the organoclay had absorption peaks at 2,925 and 2,848 cm^{-1} (oscillation of C—H bond of HB) and at 1,440 and 690 cm^{-1} (characteristic of phenyl moiety of HB) that were absent from the spectrum of pure clay [25]. These experimental results confirmed qualitatively that HB-modified clay had been synthesized.

The nanocomposites were prepared by the in situ intercalation polymerization of TPA, EG, 1,3/1,4-CHDM, and organoclay. Table 1 lists all of the compositions, viscosities, and thermal properties of the PETG/organoclay nanocomposites. The determination of the intrinsic viscosity indicated that all samples had similar molecular weights, since their intrinsic viscosities were between 0.60 and 0.63 dl/g, which range was consistent with the literature on PET nanocomposites [24, 25]. The chemical structures of the PETG were obtained by ^{1}H NMR spectroscopy. The ^{1}H NMR analysis clearly revealed that the composition of the resulting copolymer was approximately the same as that of the theoretical composition from which it was generated [9, 10].

X-Ray Diffraction

Figure 2 presents the X-ray diffraction (XRD) spectra of clay, organoclay, PETG, PETG/organoclay nanocomposites, and PET. Bragg's equation yields the interlayer spacing (d) [6, 12, 16]. From Fig. 2a, the d_{001} reflections of the clay and organoclay were $2\theta = 6.84°$ ($d =$

 DOI 10.1002/pc

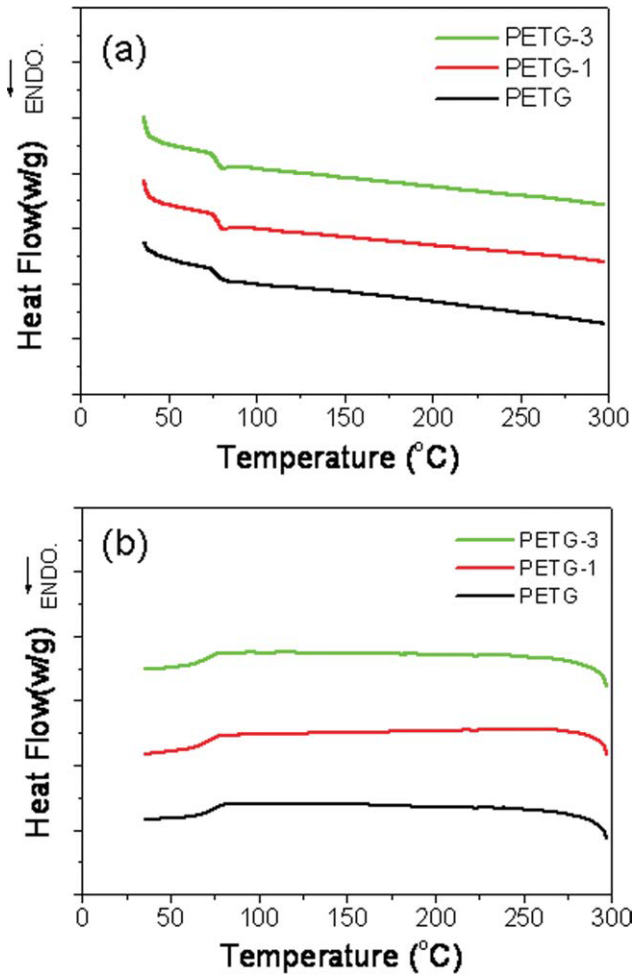

FIG. 4. DSC thermograms of PETG, PETG-1, and PETG-3: (a) second heating and (b) first cooling. [Color figure can be viewed in the online issue, which is available at wileyonlinelibrary.com.]

1.29 nm) and 2.52° (d = 3.53 nm), respectively, suggesting that the intercalation agent HB increased interlayer spacing in the clay [24, 25]. The organoclay was also observed to have a peak at 2θ = 4.90° (d = 1.80 nm), which was associated with the d_{002} reflection [6, 11–15, 21, 22]. The comparison of the XRD results for PETG nanocomposites with that of oranoclay in Fig. 2a revealed that only one of the two peaks from organoclay was obtained from the PETG nanocomposites; it was at 2θ = 4.78°, corresponding to the d_{002} reflection of the organoclay in the PETG nanocomposites. The other peak, the d_{001} reflection peak at 2θ = 2.52° from organoclay, was not detected from the PETG nanocomposites, suggesting that organoclay was intercalated and partially exfoliated by polymer chains. The intensities of the XRD peaks at 2θ = 4.78° increased with the clay loadings, indicating that PETG nanocomposite with a lower clay loading was better dispersed than that with a higher clay loading [11, 15, 21–25]. The dispersion of organoclay in the polymer matrix was further analyzed by TEM.

Figure 2b shows the XRD results for PET, PETG, and PETG/organoclay nanocomposites in the range 2θ = 10–35°. Three highly intense reflections that were characteristic of the triclinic structure of PET were observed, at 2θ values of about 17.0°, 22.8°, and 26.2° [9, 10]. The PETG and PETG/organoclay nanocomposites yielded broad amorphous X-ray diffraction patterns, indicating that the addition of organoclay to PETG did not influence the non-crystalline (amorphous) behavior of PETG.

Morphology

Figure 3 presents TEM photographs of the nanocomposites (PETG-1 and PETG-3) under different magnifications. The organoclay was well dispersed in the polymer matrix (Fig. 3a and c), although some parts of the agglomerated layers were still present on a scale of several hundreds of nanometers (Fig. 3b and d). The peak at 2θ = 4.78° in the XRD pattern of these samples may be associated with from these agglomerated layers. Furthermore, PETG-3 had more and denser agglomerated structures than PETG-1, which result was consistent with the fact that the XRD reflection profile of PETG-3 at 2θ = 4.78° was stronger than that of PETG-1. Based on the above results, the dispersion morphology of PETG/organoclay nanocomposites can be

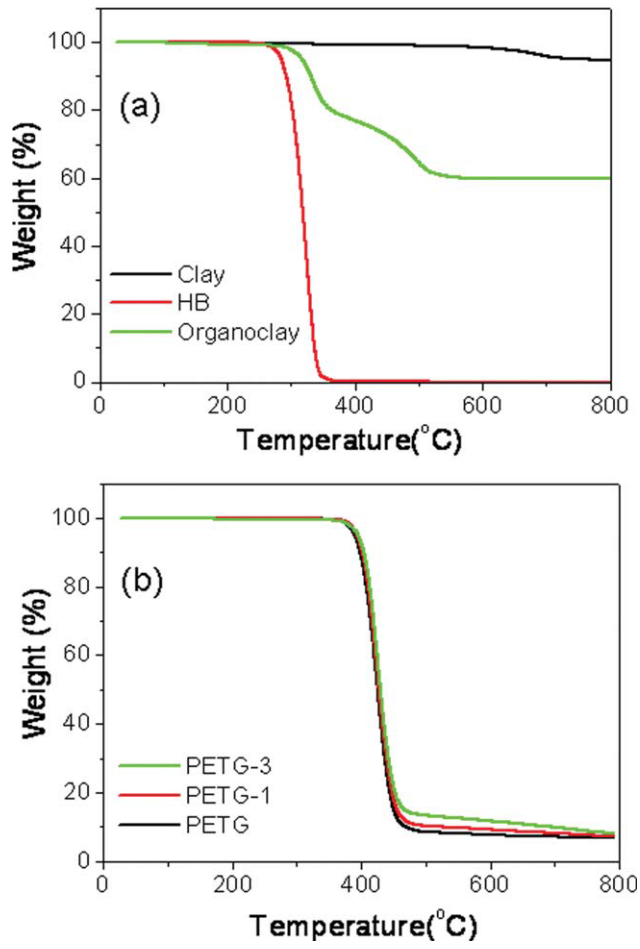

FIG. 5. TGA thermograms of (a) HB, clay, and organoclay; (b) PETG nanocomposites. [Color figure can be viewed in the online issue, which is available at wileyonlinelibrary.com.]

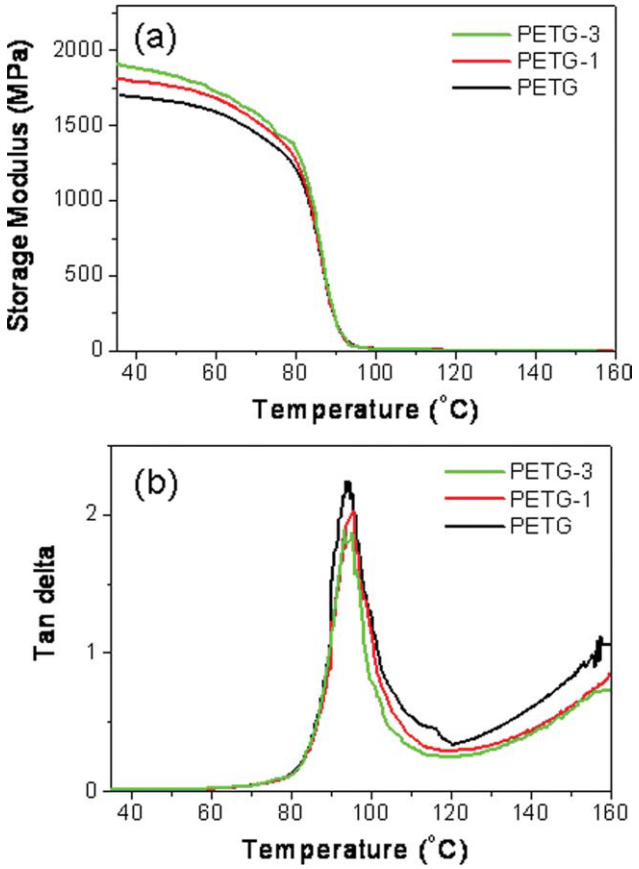

FIG. 6. DMA thermograms of PETG and PETG nanocomposites. (a): storage modulus; (b): tangent delta value. [Color figure can be viewed in the online issue, which is available at wileyonlinelibrary.com.]

considered to be a mixture of intercalated and partly exfoliated structures; a nanocomposite with a lower organoclay content may exhibit better dispersion [11, 15, 24, 25].

Thermal Properties

Table 1 summarizes the thermal properties of PETG and PETG/organoclay nanocomposites obtained using TGA and DSC. The base polymer, PETG, was amorphous, because introducing 30 mol% noncrystallizing comonomer units, 1,3/1,4-CHDM, into the crystal structure resulted in the formation of defects, which increased the crystal surface energy. Furthermore, PETG nanocomposites remained amorphous, indicating that introducing organoclay into the PETG hardly affected the crystallization rate or the crystallinity of PETG. The DSC analysis was consistent with the XRD results. The T_g of the PETG nanocomposites was almost independent of the organoclay content. Figure 4a and b plot DSC thermograms of PETG and PETG/organoclay nanocomposites during both heating and cooling at a rate of 20°C/min, respectively.

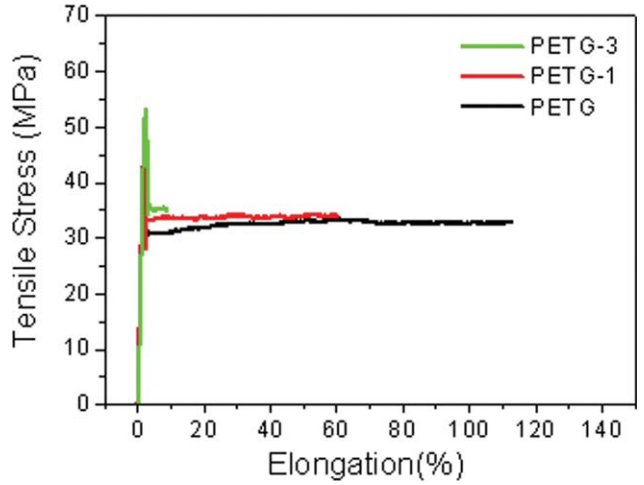

FIG. 7. Stress–strain diagrams of PETG and PETG nanocomposites. [Color figure can be viewed in the online issue, which is available at wileyonlinelibrary.com.]

Figure 5a presents the thermal stability of clay, HB, and organoclay, determined using TGA in an atmosphere of nitrogen. All of these samples started to degrade at temperatures of over 300°C; the decomposition temperature at 5% weight loss of the organoclay was 317°C, indicating that organoclay did not thermally degrade during in situ intercalation polymerization at 280°C. Figure 5b plots the TGA traces of PETG, PETG-1, and PETG-3; Table 1 summarizes these results. The thermal stabilities of these samples increased slightly with the amount of organoclay. This increase in thermal stability can be attributed to the high thermal stability of the clay and to the interactions between the clay particles and the polymer matrix [21, 22, 24, 25]. The wt% of the residue at 800°C increased with clay content. The high heat resistance of the clay was responsible for this increase in the char formation [21, 22].

TABLE 2. Dynamic mechanical and tensile mechanical properties of nanocomposite.

	Dynamic mechanical properties				Tensile mechanical properties				
	Storage modulus (MPa)								
Sample	40°C	70°C	100°C	Tan delta $T_{g\alpha}$ (°C)	Young's modulus (Mpa)	Yield stress (Mpa)	Tensile strength at break (Mpa)	Elongation at break (%)	Type[a]
PETG	1,686	1,447	12	94.4	1,849	47.9	32.9	112.9	HT
PETG-0.5	1,745	1,502	12	94.5	1,953	48.6	33.5	104.5	HT
PETG-1	1,792	1,529	13	94.5	2,099	50.8	34.0	60.1	HT
PETG-3	1,882	1,584	13	94.5	2,154	53.3	34.9	9.2	HB

[a] HT, hard and tough; HB, hard and brittle.

DOI 10.1002/pc

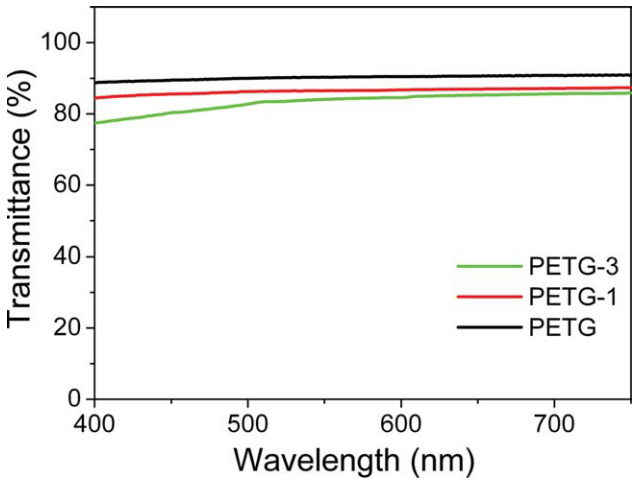

FIG. 8. Optical transmittance of PETG and PETG nanocomposites. [Color figure can be viewed in the online issue, which is available at wileyonlinelibrary.com.]

Dynamic Mechanical and Tensile Properties

Figure 6a and b plot the temperature-dependence of the storage modulus (E') and the tangent delta (tan δ), respectively. Table 2 summarizes the numerical results. All of the nanocomposites exhibited higher E' values than PETG because of the rigidity of clay; the enhancement increased with clay content (Fig. 6a). Furthermore, the intensity of the α relaxation peak of PETG nanocomposites decreased as the amount of organoclay increased (Fig. 6b), indicating that the motion of the PETG chain was constrained by the added organoclay [11, 23]. The $T_{g\alpha}$ of PETG nanocomposites measured from the peak of the tangent delta was consistent with T_g obtained from DSC, in which the T_gs of the PETG nanocomposites were almost independent of the organoclay loading and approximately equal to that of PETG.

Table 2 presents the tensile properties of the PETG nanocomposites. The tensile modulus and strength of the nanocomposites increased with the amount of organoclay in the polymer matrix, since the clay was rigid and had a high aspect ratio. However, the elongation at break markedly declined and the PETG nanocomposite, therefore, became brittle at an organoclay content of 3 wt%. This finding was consistent with the general observation that the introduction of organoclay into a matrix polymer increased its strength and modulus, but reduced its elongation at break [15, 22]. Figure 7 plots the stress–strain traces of PETG and PETG nanocomposites.

TABLE 3. Optical transmittance and gas transport properties of nanocomposites.

Sample	Transmittance at $\lambda = 400$ nm (%)	Oxygen transmission rate (mm cc/m^2 day)
PETG	88.7	12.50
PETG-0.5	86.8	8.15
PETG-1	84.4	7.60
PETG-3	77.4	6.04

Optical and Gas Transport Properties

The optical property of PETG nanocomposites was evaluated by measuring the transmittance of UV-visible rays through a sample. A higher UV-ray transmittance corresponded to a better optical property of the sample. In general, transparent polymer composites can be prepared if the polymer itself is transparent, the dispersion dimension of the fillers is smaller than one-fourth of the wavelength of visible light (390–780 nm) and the refractive index of fillers is close to that of the matrix polymer [3–5]. As the addition of organoclay did not cause PETG to generate crystalline domain, which caused the polymer to become opaque, and the organoclay was well dispersed in the polymer matrix in nanoscale, PETG nanocomposites showed the good optical property, as presented in Fig. 8.

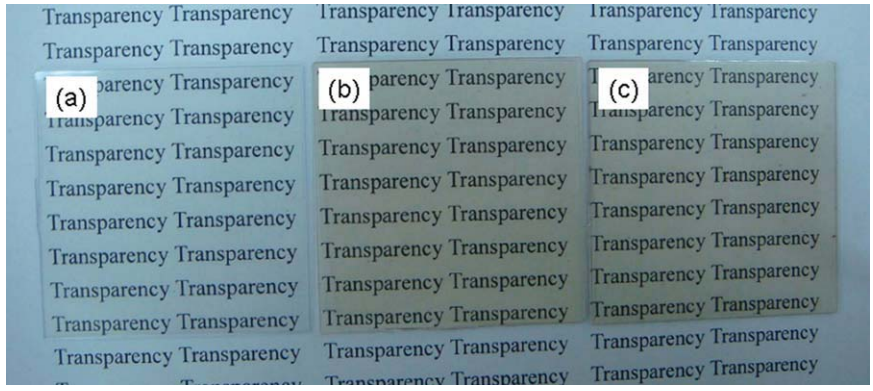

FIG. 9. Photographs of (a) PETG, (b) PETG-1, and (c) PETG-3. [Color figure can be viewed in the online issue, which is available at wileyonlinelibrary.com.]

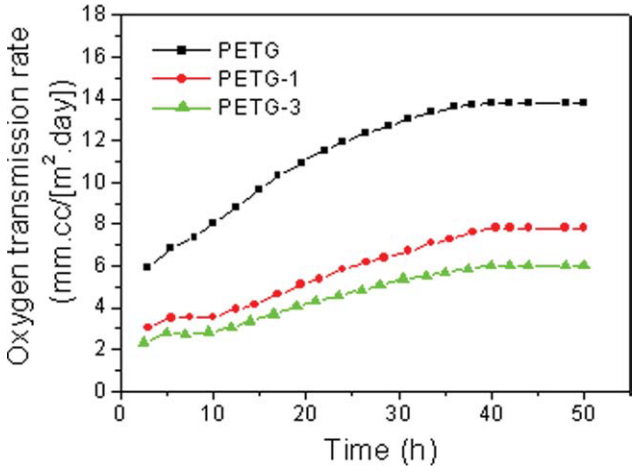

FIG. 10. Oxygen transmission rates of PETG and PETG nanocomposites. [Color figure can be viewed in the online issue, which is available at wileyonlinelibrary.com.]

Table 3 presents the specular light transmission values at $\lambda = 400$ nm. PETG was an amorphous polymer and its transmittance at $\lambda = 400$ nm was about 88.7%. The optical transmittances of PETG nanocomposites decreased with increasing the loading of clay into the polymer. This may be caused by the refractive index contrast between clay and the surrounding PETG [28], since the refractive index of PETG is 1.570 and that of clay is 1.505 [5]. However, the optical transmittances of PETG-0.5, PETG-1, and PETG-3 remained 86.8%, 84.4%, and 77.4%, respectively. Figure 9 shows photographs of PETG, PETG-1, and PETG-3 film (thickness, 0.5 mm).

The gas transport property was evaluated by measuring the oxygen transmission rate (OTR) of a polymer sheet [2, 17]. Table 3 and Fig. 10 compare the OTRs of PETG and PETG nanocomposites. The OTR of PETG nanocomposites decreased as the amount of organoclay increased. The OTR of PETG-3 was about 50% of PETG. The mechanism of the improvement on gas barrier properties is suggested to involve an increase in the tortuosity of the diffusive path of a penetrating molecule [1, 2, 17].

CONCLUSIONS

In this study, a thermally stable organoclay was used in the in situ intercalation polymerization of TPA, EG, and 1,3/1,4-CHDM to form a PETG nanocomposite. The organoclay was well dispersed in the PETG matrix, although some parts of the agglomerated layers remained on the scale of several hundreds of nanometers. Organoclay improved thermal stability, mechanical properties, and the gas transport property. The PETG nanocomposites were all amorphous and transparent. The OTR of the nanocomposite that contained 3 wt% of organoclay was about 50% of the PETG base polymer. These nanocomposites are suitable for applications that require transparency and a high gas barrier.

ACKNOWLEDGMENTS

This work was partially supported by a grant from China Medical University (CMU97-220).

REFERENCES

1. G. Choudalakis and A.D. Gotsis, *Eur. Polym. J.*, **45**, 967 (2009).
2. C. Thellen, S. Schirmer, J.A. Ratto, B. Finnigan, and D. Schmidt, *J. Membr. Sci.*, **340**, 45 (2009).
3. S.L. Hsu, U. Wang, J. King, and J. Jeng, *Polymer*, **44**, 5533 (2003).
4. T. Tsai, C. Wen, H. Chuang, M. Lin, and U. Ray, *Polym. Compos.*, **30**, 1552 (2009).
5. S. Wang, Y. Zhang, W. Ren, Y. Zhang, and H. Lin, *Polym Test.*, **24**, 766 (2005).
6. Y.H. Kim and D.S. Kim, *Polym. Compos.*, **30**, 926 (2009).
7. J.M. Lee and D.S. Kim, *Polym. Compos.*, **28**, 325 (2007).
8. S.R. Turner, *J. Polym. Sci. Part A: Polym. Chem.*, **42**, 5847 (2004).
9. Y. Tsai, C. Fan, C. Hung, and F. Tsai, *J. Appl. Polym. Sci.*, **104**, 279 (2007).
10. Y. Tsai, C. Fan, C. Hung, and F. Tsai, *J. Appl. Polym. Sci.*, **109**, 2598 (2008).
11. R.A. Kalgaonkar and J.P. Jog, *J. Polym. Sci. Part B: Polym. Phys.*, **41**, 3102 (2003).
12. R.A. Kalgaonkar and J.P. Jog, *J. Macromol. Sci. Part B: Phys.*, **B43**, 421 (2004).
13. R.A. Kalgaonkar, S. Nandi, S.S. Tambe, and J.P. Jog, *J. Polym. Sci. Part B: Polym. Phys.*, **42**, 2657 (2004).
14. R.A. Kalgaonkar and J.P. Jog, *J. Polym. Sci. Part B: Polym. Phys.*, **46**, 2539 (2008).
15. A. Ranade, N. D'souza, C. Thellen, and J.A. Ratto, *Polym. Int.*, **54**, 875 (2005).
16. H. Couderc, L. Delbreilh, A. Saiter, J. Grenet, N. De Souza, and J.M. Saiter, *J. Non Cryst. Solids*, **353**, 4334 (2007).
17. S.H. Kim and S.C. Kim, *J. Appl. Polym. Sci.*, **103**, 1262 (2007).
18. T. Wan, L. Chen, Y.C. Chua, and X. Lu, *J. Appl. Polym. Sci.*, **94**, 1381 (2004).
19. G. Guan, C. Li, X. Yuan, Y. Xiao, X. Liu, and D. Zhang, *J. Polym. Sci. Part B: Polym. Phys.*, **46**, 2380 (2008).
20. C.I.W. Calcagno, C.M. Mariani, S.R. Teixeira, and R.S. Mauler, *Polymer*, **48**, 966 (2007).
21. J.H. Chang, S.J. Kim, Y.L. Joo, and S. Im, *Polymer*, **45**, 919 (2004).
22. J.H. Chang and M.K. Mun, *Polym. Int.*, **56**, 57 (2007).
23. Y. Imai, Y. Inukai, and H. Tateyama, *Polym. J.*, **35**, 230 (2003).
24. G. Guan, C. Li, D. Zhang, and Y. Jin, *J. Appl. Polym. Sci.*, **101**, 1692 (2006).
25. X. Yuan, C. Li, G. Guan, X. Liu, Y. Xiao, and D. Zhang, *J. Appl. Polym. Sci.*, **103**, 1279 (2007).
26. Y. Tsai, L. Jheng, and C. Hung, *Polym. Degrad. Stab.*, **95**, 72 (2010).
27. Y. Tsai, C. Fan, C. Hung, and F. Tsai, *Eur. Polym. J.*, **45**, 115 (2009).
28. Y. Maruhashi and S. Iida, *Polym. Eng. Sci.*, **41**, 1987 (2001).

 DOI 10.1002/pc